Summer 2023

Impact of Dam Height and Grain Size Distribution on Breaching of Non-cohesive Dams Due to Overtopping

Heather O'Donal

IMPACT OF DAM HEIGHT AND GRAIN SIZE DISTRIBUTION ON BREACHING OF NON-COHESIVE DAMS DUE TO OVERTOPPING

by

Heather O'Donal

Bachelor of Science in Engineering
University of South Carolina, 2022

Submitted in Partial Fulfillment of the Requirements

For the Degree of Master of Science in

Civil Engineering

College of Engineering and Computing

University of South Carolina

2023

Accepted by:

Dr. Enrica Viparelli, Major Professor

Dr. Hanif Chaudhry, Committee Member

Dr. Jasim Imran, Committee Member

Ann Vail, Dean of the Graduate School

ACKNOWLEDGEMENTS

Thank you to the post-doctoral researcher Matt Czapiga, master's student Edwin Kotey, as well as undergraduate researchers who helped in construction of experiments as well as data processing, Eduardo Alvarado, Luke Groth, Our-Ntui Nikiri, Lylie Wilkie, Lauren Zalla, Megan Smith. The U.S Army Engineer Research and Development Center funded this research.

ABSTRACT

The National Inventory of Dams reports 74,400 earthen dams in the United States in 2021, of these dams approximately 27% are considered at high or significant hazard risk, that is dam failure will cause widespread damage and loss of lives. The most frequent cause of dam failure is breaching caused by overtopping. Accurate predictions of breach evolution are thus crucial to determine flood hydrographs for the safety of communities and properties at risk. Laboratory experiments were conducted on non-cohesive, compacted embankments to understand the role of dam height and sediment grain size on breaching caused by overtopping. Dam heights varied from 10 cm to 45 cm. Model structures were built with fine sand or with a mixture of fine sand and silt. Experiments showed that increasing dam height increases peak discharge. The presence of silt in model embankment material, on the contrary, lowers peak discharge and makes failure longer. In sand dams, sediment deposition on the downstream face becomes important as dam height increases. This deposition reduces incision rate of the breach channel delaying time to peak and rapid channel widening. In all embankments, breach evolution was gradual until erosion of the breach channel reached the reservoir. Throughout the experiment, bank failure caused gradual widening of the breach channel. In presence of silt, no sediment deposition occurred on the downstream face and time to peak increased with dam height because upstream migrating erosional waves formed in the breach channel and the time for these waves to reach the reservoir increased with dam height. Breach channel widening associated with bank failure is practically non-existent until peak discharge is reached, then

sudden widening caused by major failures occurs. Overall, breach width decreases with an increase in silt content.

TABLE OF CONTENTS

Acknowledgements iii

Abstract iv

List of Figures viii

Chapter 1: Introduction 1

Chapter 2: Overview of Experiments 3

Subsection 2.1: Procedures 5

Chapter 3: Results 8

Subsection 3.1: Breach Evolution in Sand Dams 8

Subsection 3.2: Dam Height Effects on Breaching of Sand Dams 10

Subsection 3.3: Breach Evolution in Sand-Silt Dams 12

Subsection 3.4: Dam Height Effect on Breaching of Sand-Silt Dams 13

Subsection 3.5: Effects of Silt Content on Breach Evolution 14

Chapter 4: Discussion 18

Chapter 5: Conclusions 22

References 24

Appendix A: Tables 25

Appendix B: Figures 27

LIST OF FIGURES

Figure B.1: Experimental Set Up 27
Figure B.2: Grain Size Distributions 28
Figure B.3: Bulk density Results 28
Figure B.4: Temporal Incision of Compaction Experiments 29
Figure B.5: Breach Hydrograph of Compaction Experiments 29
Figure B.6: Breach Evolution of 30 cm Sand Dam 30
Figure B.7: Temporal Bank Lines of 30 cm Sand Dam 31
Figure B.8: Breach Hydrograph of Reservoir Impact 31
Figure B.9: Breach Hydrograph of Sand Dams 32
Figure B.10: Temporal Incision of Sand Dams 32
Figure B.11: Temporal Width of Sand Dams 33
Figure B.12: Breach Evolution of 30 cm Dam with 25% Silt Content 34
Figure B.13: Temporal Bank Lines of 30 cm Dam with 25% Silt Content 35
Figure B.14: Breach Hydrograph of 25% Silt Content Dams 35
Figure B.15: Temporal Incision of 25% Silt Content Dams 36
Figure B.16: Temporal Incision of 30 cm Dams all Grain Sizes 36
Figure B.17: Temporal Width of 30 cm Dams all Grain Sizes 37
Figure B.18: Temporal Top Width in all Locations of 30 cm Dams all Grain Sizes 37
Figure B.19: Breach Hydrograph of 30 cm Dams all Grain Sizes 38
Figure B.20: Non dimensional Breach Hydrograph of Repeated Experiments 38

Figure B.21: Temporal Incision of Repeated Experiments 39

CHAPTER 1

INTRODUCTION

The National Inventory of Dams (2021) reports 74,400 earthen dams in the United States, and of those dams approximately 27% are at high or significant risk hazard potential. This means that if failure were to occur, property damage or even loss of life will occur. Specifically, the most common failure type of earthen dams is breaching due to overtopping which accounts for 34% of all failures (2022). These failures occur in dams of different sizes and built with different materials, parameters that play a role in breach formation and development. Understanding how dam size and material impact breach evolution is thus crucial to characterize and predict failures for the safety of citizens and properties surrounding earthen dams.

A review of the literature reveals that the impact of sediment properties and dam size on breach evolution in non-cohesive, compacted dams remains poorly characterized due to process complexity and difficulties in scaling hydraulically relevant material properties. Experiments were performed to understand the role that compaction and compaction-related soil properties, sediment gradation and initial breach geometry have on breaching in non-cohesive dams. Tabrizi et al. (2017) conducted laboratory tests on non-cohesive dams and the effect that compaction has on breaching caused by overtopping. These experiments showed that peak discharge decreased with compaction level, while time to peak increased (Tabrizi et al., 2017).

Mohamed & El-Ghorab (2016) performed laboratory tests on scaling of non-cohesive embankments. It was found that breach channels in large embankments (1.8 m tall) and small embankments (1:2 and 1:4 the scale of the large) had similar geometry and rate of breach evolution. Walder et al. (2015), however, showed how increasing dam height resulted in increased peak discharge. Further, the same experiments demonstrated that breach hydrographs were similar in shape after a certain time regardless of initial dam height. Schmocker & Hager (2012) performed laboratory tests to investigate the impacts of dam height and sediment size on plane dike breach due to overtopping and concluded that erosion is fastest in small dams. The same authors also noted that in early stages of breaching erosion is fastest in embankments built with coarse sediment due to highest saturation. As breach develops, however, breach development is slowest in coarse sediment dams because erosion is governed by bedload transport and coarse sediment is harder to transport than fine material (Schmocker & Hager, 2012).

Experiments on overtopping of non-cohesive dams with gravel in the sediment gradation showed that the initial rate of breach deepening is greater than the rate of breach widening (Coleman et al., 2002). Chinnarasri et al. (2004) used a mixture of 70% coarse sand and 30% clay that had a median grain size of 0.06 cm, as well as a mixture of 70% fine sand and 30% clay that had a median grain size of 0.034 cm and observed that breach evolution was first characterized by channel deepening followed by widening. These experiments further showed that increasing the median grain size diameter, through the inclusion of fine sand, increased the peak outflow (Chinnarasri et al., 2004). Similar finding are reported in Pickert et al. (2011) for laboratory experiments with homogeneous, non-cohesive embankments, coarse material experiences vertical and transverse erosion whereas

breaching in dams built with fine material was primarily characterized by vertical erosion. Further, Pickert et al. (2011) observed that channel incision occurred with erosion rates that did not change in time in dams built with coarse material while erosion rates were variable in model embankments made of finer sediment. Channel widening in the same experiments occurred with relatively frequent and small bank failures in coarse dams and with episodic and large mass failures (Pickert et al., 2011). Finally, Cestero et al. (2014) performed experiments on the effect of soil properties such as gradation and cohesion, bulk density, and moisture content, in the development of levee breaches caused by overtopping and found that the inclusion of silt reduced peak discharge and breach evolution time.

In this thesis, results of experiments specifically designed to explore effects of dam height and sediment grain size distribution on evolution of a breach channel in non-cohesive dams are presented. Breaching caused by dam overtopping is analyzed in terms of breach widening, deepening, and time between the beginning of dam overtopping and the occurrence of peak breach discharge (time to peak). Embankment height varied between 10 cm and 45 cm. Embankment material consisted of non-uniform sand and of two mixtures of this sand with silica flour, i.e., material in the silt range. The experimental plan is presented in Chapter 2 and is followed by a detailed description of the experimental set up and procedure. Breach evolution results are then presented for sand dams of varying heights and for sand-silt dams with varying silt content. A discussion of how experimental results presented here compare with previous studies is followed by a section summarizing the main conclusions of the study. The entire dataset and the Supplementary Videos are available at doi:10.5061/dryad.cvdncjt8k.

CHAPTER 2

OVERVIEW OF THE EXPERIMENTS

Experiments were performed in the Hydraulics Laboratory of the Department of Civil and Environmental Engineering at the University of South Carolina, Columbia, in a 15 m long, 1 m wide and 1 m deep flume schematically illustrated in Figure 1 with the measurement devices used to characterize breach evolution in time. A 0.4 m tall and 5 m long wooden platform was installed to create a settling basin downstream of the dam and collect sediment before it reached the laboratory sump. Dams were built on this wooden platform.

All dams were built the full flume width, with 0.3 m long crests and 3:1 slope (H:V) of the upstream and downstream faces. The upstream toe of the dam was positioned 0.5 m downstream of the platform edge, as shown in Figure 1. A constant inflow discharge of 4.5 l/s was supplied to the reservoir with a sump pump (Figure 1) and a sharp-crested weir directed flow out of the reservoir to maintain a constant reservoir head.

Grain size distributions of three sediment mixtures used in the experiments are presented in Figure 2 along with the grain size distribution of the silica flour. Standard sieve analysis was performed to measure the grain size distribution of the sand and a H151 soil hydrometer was used to measure the grain size distribution of sediment in the silt range. The grain size distribution of the silica flour presented in Figure 2 was given by the manufacturer. Sand-silt mixtures were obtained by adding 10% and 25% silica flour by volume to the sand. The blue line in Figure 2 represents the sand used in the baseline tests.

This sand has geometric mean diameter D_g equal to 0.39 mm, geometric standard deviation σ_g = 1.93, a median grain size D_{50} = 0.39 mm, D_{10} = 0.15 mm, D_{90} = 0.96mm, with D_{10} and D_{90} respectively denoting sediment sizes such that 10 and 90 percent of the sediment is finer. Standard proctor test was used to determine the optimum moisture content for the sand at 5%. The geometric mean diameter D_g of the silica four is equal to 0.02 mm and the geometric standard deviation σ_g = 28.55.

The orange line in Figure 2 represents the coarsest sand-silt mixture, which was obtained by adding 10% by volume of silica flour to the original sand. This resulted in a sediment mixture with D_g = 0.28 mm, σ_g = 3.32, D_{50} = 0.49 mm, D_{10} = 0.07 mm, D_{90} = 0.93 mm, and optimum moisture content 7%. The grey line in Figure 2 represents the finest sediment mixture obtained by mixing 25% by volume of silica flour and 75% of the sand. Characteristic diameters of this sediment mixture are D_g = 0.18 mm, σ_g = 4.98, D_{50} = 0.30 mm, D_{10} = 0.0074 mm, D_{90} = 0.87 mm, and an optimum moisture content of 9%.

Dams were built with heights of 10 cm, 15 cm, 20 cm, 30 cm, and 45 cm, as summarized in Table 1 where experiments are presented in terms of dam height and sediment type. Experiments were first performed with sand dams of five different heights to evaluate the impact that dam height has on breach evolution in non-cohesive dams. Three dam heights (15 cm, 20 cm, and 30 cm) were then used to evaluate the impact of sediment size and height in increasing silt content. An additional 13 experiments were conducted to check that the experiments were repeatable. Repeatability plots are presented in the thesis appendix and the data are included in the publicly available dataset.

2.1 PROCEDURES

Prior to dam construction, water was added to sand in a concrete mixer to achieve the optimum moisture content in the experiments with sand dams. In the sand-silt experiments, silica flour was mixed with a portion of water in advance to prevent the spreading of fine particles in the lab. Sand and water were then mixed, and the silica-water mix was then added into the concrete mixer to obtain a sediment mixture with the optimum moisture content.

Sediment was placed into the flume in lifts of approximately 7cm in height. A stair-shaped framework on the flume sidewalls and pieces of wood used along the width of the flume were used to help contain sand during compaction. Each lift was evenly compacted with 10 blows of a hand tamper to achieve a compacted lift of 5 cm and repeated until the final dam height was achieved. Once the final dam height was reached, sides were shaved to the desired 3:1 slope. A 2 cm wide by 1.9 cm deep rectangular pilot channel was cut through the center of the dam crest, to direct the breach through the center and prevent any effect of the flume side walls.

Chalk was used to make a grid on the downstream face and on the dam crest. Horizontal chalk lines were drawn every 5 cm in elevation from the toe to the downstream crest. Two horizontal lines were placed on both the upstream and downstream ends of the dam crest. Vertical lines were drawn every 10 cm. These grid lines were used to determine the width of the breach, as well as determining the location that sediment deposition or erosion was occurring.

Four experiments were performed to test the impact of and determine the level of compaction needed for experiments, experiments 2, 13,14, and 15 in Table A.1. Different numbers of blows for compaction as well as cumulative compaction of sediment layer were tested to study the impact of compaction on bulk density, results presented in Table A.3 and Figure B.3. The maximum bulk density was achieved after about 15 blows on one layer or 15 cumulative blows on multiple layers and increasing the number of blows beyond this point had no additional effect (Figure 3). In the experiments presented herein 10 blows of compaction per layer were used therefore after 2 layers, which all dams had three plus players, maximum bulk density was achieved. These results of the bulk density test explain why when dams with different blows of compaction performed with cumulative layers in our experiments show similar erosion and breach hydrograph (Figure 4 and 5).

A sonar probe and a point gauge were used in the reservoir to measure water level (Figure 1) throughout the entire experiment and was used to compute breach hydrographs. The elevation of water level over the elevation of the weir crest, also known as the head over the weir, was used to compute the discharge going over the weir. This weir discharge was then used in conjunction with the known inflow discharge to compute the breach discharge as inflow discharge subtracted by weir discharge.

Breach erosion on dam crest was measured 10 cm upstream of the downstream edge of the crest with a Keyence laser profiler LJ-V7200 (Figure 1). The laser emits a beam to the dam crest and receives reflected light. Based on the change in the position where the light is received back into the laser, the sensor can detect the change in the distance to the dam crest. A MATLAB code was developed and used to convert laser outputs into temporal data for elevation on the dam crest.

Two cameras monitored spatial and temporal changes in breach width. One camera was placed downstream of the dam to image the downstream dam face and a GoPro camera was placed just upstream of the dam to image the dam crest (Figure 1). Frames were extracted from the video recordings and manually digitized the dam geometry throughout the experiment. This digitized data could then be processed into temporal width data at varying locations along the downstream dam face and crest.

At the beginning of each experiment the reservoir was filled with a pump until water began flowing over the weir. The reservoir level continued to rise until water began flowing through the pilot channel. The moment when the water enters the channel is used as time equal to 0 in all experiments, thus negative times refer to measurements collected before water entered the pilot channel. Experiments ended when the water level in the reservoir dropped to a constant level at which point the breach discharge had also reached a constant rate.

CHAPTER 3

RESULTS

In this chapter breach evolution in sand dams is described in section 3.1. The impact of changing dam height on breach development in compacted sand dams is discussed in section 3.2. Breach evolution in sand-silt dams is described in section 3.3, followed by the impact of changing dam height in sand-silt dams in section 3.4. The comparison between breach evolution in sand and sand-silt dams is presented 3.5.

3.1 BREACH EVOLUTION IN SAND DAMS

Breach evolution for a 30 cm high sand dam is presented in Figure 6 and Supplementary Video 2. Breaching of sand dams is divided in three phases. Phase 1 begins when water enters the pilot channel (Figure 6a), entrains and transports sediment and deposits it on the downstream face of the dam. Phase 1 ends when the flow reaches the dam toe, and incision of the breach channel begins (Figure 6b). In phase 2 incision of the breach channel occurs. This incision starts in the downstream part of the dam face and migrates upstream. Sediment is deposited near the dam toe. As time passes, channel incision eventually reaches the dam crest with no major change in breach discharge (Figure 6c). Phase 2 ends when the incision reaches the upstream limit of the dam crest, i.e. the reservoir.

In phase 3 the upstream end of the dam crest is eroded, breach discharge and sediment erosion rates rapidly increase, sediment is transported downstream of the dam toe allowing erosion of the lower part of the downstream dam face. In response to the increased incision

rate of the breach channel, bank failure become more frequent causing a continued gradual widening of the breach channel (Figure 6d), this widening can be seen in Figure 7 which maps the left and right banks of the channel at various times throughout the experiment. Dashed lines in Figure 7 show the locations of the dam toe, and dam crests, and color represents the difference in time with blue being time 0 and red being the end of the experiment.

Bank failures occurring at this stage are initiated in the downstream part of the breach channel and cause bank failure to propagate upstream. As breach channel widens, breach discharge increases until the entire height of the dam is eroded, the platform is exposed near the dam toe (arrow in Figure 6e) and soon after the peak discharge occurs (Figure 6f). At this point, undercutting and instability in the banks result in larger bank collapses (Figure 6g) and the final breach width at the end of the experiment (Figure 6h). Breach evolution in terms of timing of the three phases is presented in Table 2, with information on the relevant events. Specifically, all experiments start at time 0s and the second column in the table shows the time that phase 1 ends and water reaches the dam toe. The third column shows the time that the second phase ends and the upstream crest of the dam is eroded. Columns 4 and 7 show times where either minor or major bank failures occur causing changes in the channel width, not all experiments experience such failures and thus the column could be left blank. Column 5 shows the time the dams' height is eroded and the platform is exposed, this occurs before or at a very similar time to the time that the peak discharge occurs as shown in column 6. Lastly column 8 shows the time the experiment is concluded.

3.2 DAM HEIGHT EFFECTS ON BREACHING OF SAND DAMS

Before discussing the impact of dam height, the impact of reservoir volume alone is first considered because the reservoir volume increases with dam height. To determine how the increasing reservoir volume with constant dam height impacts breach hydrograph, run 2 was repeated with same conditions except a larger reservoir in run 12. Breach hydrographs of runs 2 and 12 are compared in Figure 8 in terms of ratio between breach discharge and inflow discharge, with the shaded area representing the impact of reservoir volume. Figure 8 shows how a larger reservoir volume creates a larger peak discharge and a longer time to peak. The dashed vertical lines on the graph represent the end of phase 1, and the dotted vertical line represents the end of phase 2, these phases have similar durations despite changes in reservoir size.

Experiments 1 through 5 show that increasing dam height results in larger peak discharges. This is illustrated in Figure 9, where panel a show the breach hydrographs for dams of heights equal to 10 cm, 15 cm, and 20 cm (called small dams herein) and panel b shows breach hydrographs for the 30 cm and 45 cm dams (large dams). The dashed vertical lines on this graph represent the end of phase 1, and the dotted vertical lines represent the end of phase 2.

The impact of dam height on Phase 1 is related to the competing effects of hydraulic head and sediment deposition on the downstream face (Supplementary Videos 1 and 2 showing breaching in experiments 2 and 4). The higher the dam, the more sediment deposition occurs on the downstream dam face, and this deposition tends to make phase 1 longer in tall dams, this can be seen in Column 3 of Table 2. On the other hand, the higher the dam, the higher the hydraulic head driving the flow when the breach channel reaches the dam

toe, which results in faster breaching in phase 2 (Table 2 column 4). The competition between sediment deposition and hydraulic head impacts the duration of the first two phases of breaching. More specifically, in small dams (Figure 9a and Supplementary Video 1) there is little sediment deposition on the downstream face, thus water reaches the toe relatively rapidly and breach evolution is primarily controlled by hydraulic head. Therefore, as dam height increases in the small dams the sooner phase three begins, which means the sooner rapid erosion, and time to peak occur (Figure 9a). In large dams, the initiation of the third phase is delayed by the competing effects of hydraulic head and sediment deposition on the downstream face during the first two phases (Supplementary Video 2). In these experiments, significantly more sediment deposition on the downstream face occurs compared to the experiments with small dams delaying the time for the water to reach the dam toe and the incision of the breach channel (phases 1 and 2). As a result, these dams have a much longer time for the third phase to begin, thus longer time to peak, when compared to small dams (Figure 9b).

Lastly incision and widening of breach channels also vary with dam height, as shown in Figures 10 and 11, respectively for a cross section located on the dam crest, 10 cm upstream of the downstream crest, as shown in Figure 1. Laser-based incision rates of dam crest are presented in Figure 10, where the y axis shows the depth eroded below the dam crest in centimeters, 0 on the y axis is equal to the initial elevation of the dam crest. Line slopes in Figure 10 represent channel incision rates and spikes are representative of bank failures with sediment falling into the channel. As dam height increased in small dams the rate of rapid erosion was greater due to greater hydraulic head and reservoir size. In large dams, gradual incision lasted for a much longer time, also followed by a rate of rapid incision

after the crest is eroded (Figure 10 green and purple lines). After the crest is eroded the rapid incision rate is similar for large dams as well as the 20 cm dam, as indicated by the nearly parallel slopes of the laser measurements.

Widening of dam crest 10 cm upstream of the downstream face is presented in Figure 11 where the temporal evolution of the channel width is plotted. Horizontal slopes are representative of no channel widening. The onset of channel widening is also delayed in large dams due to the relatively long phases 1 and 2 of breaching, caused by sediment deposition on the downstream face. Interestingly, phase 3 breach channels in large dams are narrower than in small dams throughout the experiment this may be attributed to the fact that the breach channel reaches the platform relatively rapidly in small dams and thus the presence of a non-erodible channel bottom induces more erosion of the channel banks. Another reason to explain the presence of wider phase 3 breach channels in small dams is that the moisture content around the breach channel is larger in small dams. In other words, the higher the dam, the longer it takes the sand surrounding the breach channel to be fully saturated and fail.

3.3 BREACH EVOLUTION IN SAND-SILT DAMS

Breach evolution of sand-silt dams is also described in terms of the three phases introduced for the sand dam experiments, as illustrated in Figure 12 and supplementary video 3 for the 30 cm high, 25% silt dam. The first phase begins as water enters the channel; breach flow immediately travels to the dam toe with very little to no sediment deposition on the downstream face (Figure 12b). As incision continues in phase 2, erosional steps develop in the breach channel causing sediment deposition at the dam toe (arrows in Figure 12c). Eventually these steps begin migrating upstream as erosional waves. As waves migrate

upstream, the channel rapidly deepened as each wave passes. The second phase of breaching is concluded when the erosional steps reach the upstream crest and phase 3 begins (Figure 12d). At the end of phase 2 sediment accumulated at the dam toe (arrow in Figure 12d) and few to no bank failures occurred, therefore little to no widening beyond the original width of the breach channel was measured this lack of widening, as shown in Figure 13 with left and right banklines of the breach channel at various times.

In phase 3 as breach discharge increases, erosional steps dissipate, and rapid incision occurs. Minor bank failures occur near the dam toe causing channel widening shown by the yellow lines near the dam toe in Figure 13. The deposit near the dam toe formed during phase causes a scour hole to develop upstream of the deposition, and results in a hydraulic jump as indicated in Figure 12e with the arrow and shown in Supplementary Video 3. The hydraulic jump causes more minor failures and channel widening upstream (Figure 12f). It is at this point that peak discharge occurs (Figure 12g). The hydraulic jump and high discharge cause bank undercutting and lateral erosion at the dam toe, which can also be seen in Figure 12g shown by the arrow. Eventually the deposited sediment in the channel is eroded and the hydraulic jump dissipates. It is after this point that the undercutting is too large, the banks become unstable and major bank failures occur resulting in sudden widening and the final breach width (Figure 12h) and shown by the red line in Figure 13.

3.4 DAM HEIGHT EFFECTS ON BREACHING OF SAND-SILT DAMS

As the height of a sand-silt dam increases, peak breach discharge increases due to increased reservoir size and hydraulic head, as illustrated in Figure 14 where the breach hydrograph for all 25% sand-silt dams is shown. In Figure 14, the 20cm dam hydrograph has two peaks caused by a major bank collapse, which momentarily prevented flow through the channel

until the collapsed sediment was eroded away. It is reasonable to assume that in the absence of bank failure, the peak of the 20 cm dam experiment would fall between the peaks of the 15 cm and 30 cm dam experiments for both time and magnitude.

In sand-silt dams, the time to peak discharge depends on the time duration of the second phase, or the time for the upstream crest to be eroded. In sand-silt dams the duration of the second phase is controlled by the speed and distance for the erosional waves to travel which is greater with increased dam height, the time of phase 2 is shown in Table 2 column 3.

Figure 15 presents the temporal evolution of breach channel depth below the initial dam crest for 15 cm, 20 cm, and 30 cm dams with 25% silt content. Arrows indicate sudden deepening of the breach channel in phase 2 corresponding to the passage of an erosional wave. The dashed vertical lines represent the end of phase 1, while the dotted vertical lines represent the end of phase 2. As dam height increases the time for the incisional step to reach the crest is greater which results in rapid incision and thus time to peak discharge to be greater as well (Figure 14).

3.5 EFFECTS OF SILT CONTENT ON BREACH EVOLUTION

The comparison between experiments performed with varying silt content ranging from no silt (experiments 1-5) to 25% silt content (6-8), and an in between case of 10% silt content (9-11) shows that breach evolution and breach discharge vary with silt content. Little or no sediment deposition is observed on the downstream face of sand-silt dams therefore the time for the flow to reach the dam toe and start incising the breach channel is significantly shorter in sand-silt dams compared to sand dams, this can be seen in Table 2 in terms of duration of phase 1 in the second column. In contrast, phase 2 corresponding to the incision

of the breach channel downstream of the upstream crest, is much longer in sand-silt dams due to the formation of erosional waves that migrated upstream until they eroded the upstream crest, column name in Table 2.

Incision of the breach channel on the dam crest for the 30 cm dams and all three sediment mixtures is presented in Figure 16. The dashed lines represent the time phase 1 ends for each experiment, it is shown by these lines that the 100% sand dam has a much longer first phase compared to the sand-silt dams. Similarly, the dotted lines show the time that phase 2 ends. For the 100% sand dams the two lines are extremely close together showing that the second phase for this dam is extremely small. In comparison, the dotted lines for the sand silt dams are at much later times which show how long the second phase of breaching is in sand-silt dams. Breach channels in compacted sand dams experience two types of erosion, a gradual vertical incision of the channel associated with some widening (phase 2) followed by rapid incision once the upstream crest is eroded (phase 3) (arrows in Figure 16). Breach channels along the dam crest in sand-silt dams, on the contrary, experience very little incision and no widening while the erosional waves are forming along the downstream face (phase 1 and 2). Once the erosional waves reach the dam crest vertical erosion occurs in steps equal to the depth of the erosional waves (Figure 15) until a wave reaches the upstream crest which then causes rapid incision to occur (phase 3). Once the upstream crest is eroded, incision rates are similar for all dam materials (arrows in Figures 16). It can be seen in Figure 16 that the 10% sand-silt dams are a mixture of the two incision processes, the crest is eroded at a similar time to sand dams, however it is eroded in step by an erosional wave.

Widening of the breach channel on the dam crest is presented in Figure 17 for 30 cm dams of all three sediment mixtures. The dashed vertical lines represent the end of phase 1, while the dotted vertical lines represent the end of phase 2. The presence of silt in dams changes the mechanism of widening. In sand-silt dams, width does not gradually increase due to bank collapses as it does in sand dams; rather, channel width is relatively constant until the upstream crest is eroded and the breach discharge is approaching the peak. It is at this point that bank failures begin to occur, and the channel begins to widen (Figure 17). Also observed with the presence of silt, as breach discharge is approaching the peak, lateral erosion is occurring at the water surface level in the breach channel causing the formation of overhanging banks whose failure results in sudden channel widening.

When comparing experiments with 10% silt content, it is observed that 10% dams have a combination of both widening mechanisms that are observed in sand dams and 25% dams. Overall channel width at the end of the experiment decreases with increasing silt content (Figure 17). Figure 18 shows the top channel width at all locations where each colored line is a different time throughout the experiment for breaching of a 30 cm dams, data in panel a pertain the 100% sand dam experiments, data of the 10% and 25 % silt experiments are respectively presented in panels b and c. The color bar on the right of each frame shows the change in color equivalent to time. These graphs show that increasing silt content results in narrower breach channels as well as the fact that failures or changes in width do not occur until later in the experiment when silt is present. These figures also show that gradual channel widening occurs downstream initially until bank failures occur which widen throughout the entirety of the channel. It is also noticed that 100% sand dams widen the channel at the location of the reservoir however this does not appear to occur in the

sand-silt dams. This channel widening at the reservoir could be attributed to the larger peak discharge in sand dams.

Lastly, Figure 19 shows breach hydrographs for 30 cm dams of all three sediment mixtures. The dashed vertical lines represent the end of phase 1, while the dotted vertical lines represent the end of phase 2. The 25% silt content dam had the lowest peak discharge, while the sand and the 10% silt content dams had similar peak discharge. This is likely a consequence of the smaller (narrower) breach channel that forms in the 25% sand-silt dam at the end of phase 2 compared to the breach channels that formed in the sand and 10% sand-silt experiments. Similarly, due to the longer phase 2, the 25% silt dams took the largest amount of time to reach peak discharge, while the time to peak in the experiments with sand and 10% sand-silt dams were more similar due to end of phase 2 occurring at similar times (Figure 19).

CHAPTER 4

DISCUSSION

Before drawing conclusions from experimental results, it is important to confirm that the experiments are repeatable and that results are comparable throughout the experiments. To ensure this, multiple experimental runs were repeated, experiments 13 – 17 in TableA.2. Specifically, three 20 cm dams of 100% sand were performed (Figure 20a), two 30cm dams of 100% sand (Figure20b), two 15cm dams of 25% silt (Figure 20c) and lastly two 15cm dams of 10% silt (Figure20d). Figure 20 shows the comparison between nondimensional breach hydrographs of repeated experiments, frames a through d show that the breach hydrographs for repeated experiments have similar shapes including time to peak and peak discharge. Figure 21 shows the comparison between time evolution of breach channel depth below the initial dam crest for the repeated experiments, with frames a through d showing the same repeated experiments as in Figure 20. Similar to the breach hydrographs, the incision in repeated experiments also has similar rates or incision patterns. In Figure 21b the blue line is missing data in the beginning because the laser was initially placed too close to the surface of the dam and could not collect data until a certain depth was reached, after this point however the incision rates on this graph are similar for all 30 cm 100% sand dams. Figures 20 and 21 show similar breach characteristics for repeated experiments, it is unlikely the results would be identical since breaching is not an exact process each time therefore the results presented show that the experiments performed are reliable.

In previous experiments Tabrizi et al. (2017) studied the effects of compaction on embankment breaching due to overtopping. Specifically, these authors concluded that in embankments with no compaction the failure mechanism was surface erosion while head cut erosion was present along with surface erosion in compacted embankments. Overall, embankment failure was faster in experiments with no compaction, peak discharge decreased and time to peak increased with compaction. The experiments performed in this paper conclude that compaction did not impact breach parameters because maximum compaction was reached in all experiments (Figures 3, 4 & 5).

Systematic studies of dam height impact on breach evolution in dams are scarce. Walder et al. (2015) performed experiments on overtopping of non-cohesive sand dams and noticed that the higher the dam, the larger the peak discharge. Similar results were obtained in the experiments described in this paper (Figure 9). Erosional steps developed along the downstream face from alternating steep and gentle gradients in the Walder et al. (2015) experiments. These steps migrated upstream and coalesced until finally reaching the upstream crest which caused rapid reservoir drainage. Erosional steps that were observed in the experiments of sand-silt dams also developed along the downstream face of the dam soon after the experiments began and, similarly to what was observed in Walder et al. (2015) experiments, migrated upstream and occasionally coalesced until reaching the crest. It is unclear whether the erosional steps formed in our experiments were caused by changes in slope as they form so soon into the experiment, where little erosion has taken place.

Schmocker & Hager (2012) studied the impact of non-compacted, noncohesive plane breached dikes and concluded that vertical erosion happened sooner in smaller dikes. However, after a certain time the eroded dike height was similar for varying heights. The

results presented in this thesis agree with the conclusion that decreasing dam height shortens the breach evolution and specifically vertical erosion occurs sooner (Figure 10). The current study however did not show that varying initial dam heights resulted in similar overall dam heights at the end of experiments. This difference can be due to the fact that Schmocker & Hager (2012) did not compact material for the dikes and did not use a pilot channel to direct the flow over the dike.

Schmocker & Hager (2012) also varied the grain size in experiments through the inclusion of gravel with homogenous sand, it was concluded that during the initial phase of breach development, the dike eroded faster with an increasing sediment diameter, due to sliding failures of larger particles coupled with higher saturation. After 10 seconds of breaching, however, erosion is governed by bedload transport with coarser materials being less mobile than fine sediment. Our experiments show that during the first phase of breaching vertical erosion is faster in sand than in sand-silt dams, as shown in Figure 16 where sand dams have gradual erosion. The processes controlling breach channel incision in our experiments are different that the bedload transport discussed by Schmocker & Hager (2012), they are associated with upstream migrating gradual erosion in sand channels, and with the formation of upstream migrating waves in the sand-silt case.

Similar to Schmocker & Hager (2012), Chinnarasri et al. (2004) performed experiments on breaching due to overtopping in embankments where the median grain size was varied through the inclusion of clay in sand dams. Main results of the experiments are that when the grain size diameter was increased the peak outflow also increased. This agrees with the results of our experiments and can be seen in Figure 19 where the sand dams have the largest peak discharge. It was also concluded that when grain size diameter was decreased

the breach deformation time increased. This again agrees with the results of the current experiments shown in Figure 19 where the finest material, the 25% sand-silt dams, have the longest time to peak.

Pickert et al. (2002) also performed experiments on breaching caused by overtopping of earthen embankments and focused on the impact of cohesion on discharge hydrograph, breach failure mechanisms and temporal breach profiles. Breach evolution was described in two phases separated by the erosion of the upstream crest, which causes increases in erosion rates as well as breach discharge. The same increase in channel incision rate and breach discharge was observed slopes were only stable due to negative pore-water pressure and suction in the embankment material. Similar overhang was observed in the 25% sand-silt experiments.

CHAPTER 5

CONCLUSIONS

The experiments presented herein indicate that the breaching of a compacted, non-cohesive embankment dam depends on the height of the dam as well as the grain size distribution of the material used in the dam. Regarding peak discharge, increase in the dam height resulted in an increase of peak discharge regardless of the sediment grain size distribution. More specifically, the finer the grain size distribution resulted in lower peak discharges.

The temporal evolution of breach discharge in sand dams is dependent on the competing effects of sediment deposition on the downstream dam face, hydraulic head and reservoir size. The former tends to delay the time for the water to reach the dam toe and thus increases the length of phase 1 of breaching. The others tend to accelerate channel erosion on the downstream slope and on the dam crest once the flow reached the toe (phase 2).

Incision in 25% silt content dams is controlled by upstream migrating erosional waves. Increasing dam height resulted in longer time for the erosional waves to reach the upstream crest and thus initiate rapid incision rates. The characteristics of erosional waves appear to depend on dam height therefore further research is needed to investigate the dynamics of the formation, speed, and depth of upstream migrating erosional waves. Overall changing the grain size distribution of dams causes changes in the incision mechanisms. Specifically,

the presence of fine material results in the formation of erosional steps that migrate upstream while coarser material experiences constant gradual and rapid incision rates.

The temporal evolution of widening that occurs in sand dams is longer as dam height increases. In all sand dams widening is similar, i.e., width is constant until a bank failure occurs then a sudden change in width results and this pattern is repeated regularly throughout the experiments. In 25% silt content dams breach channel width does not change until the peak discharge occurs, at which point the width increases suddenly. This process is dependent on height, as the height increases the time for the width to drastically increase is longer. The widening mechanism is therefore different based on the grain size distribution. Fine material experience little to no widening until the peak discharge when a sudden widening occurs whereas in coarse materials gradual steps in width occur throughout the experiments. Lastly, the overall width at the end of the experiment decreases with an increase in silt content.

REFERENCES

Chinnarasri, C., Jirakitlerd, S., and Wongwises, S. 2004. "Embankment Dam Breach and Its Outflow Characteristics". *Civ Eng Environ Syst.* 21. 247-264. DOI: 10.1080/10286600412331328622

Coleman, E. S., Andrews, D.P., and Webby, M.G. 2002. "Overtopping Breaching of Noncohesive Homogeneous Embankments.". *J. Hydraul. Eng.* 128(9): 829-838

Pickert, G., Weitbrecht, V., and Bieberstein, A. 2011. "Breaching of Overtopped River Embankments Controlled by Apparent Cohesion". *J. Hydraul. Res.,* 49:2, 143-156, DOI: 10.1080/00221686.2011.552468

Schmocker, L. & Hager, W. H., (2012). "Plane Dike-Breach Due to Overtopping: Effects of Sediment, Dike Height and Discharge". *J. Hydraul. Res.,* 50:6, 576-586, DOI: 10.1080/00221686.2012.713034

Tabrizi, A. A., Elalfy, E., Elkholy, M., Chaudhry, M. H., and Imran, J. 2017. "Effects of compaction on embankment breach due to overtopping". *J. of Hydraul. Res.*, 55:2, 236-247, DOI: 10.1080/00221686.2016.1238014

Walder, J.S., Iverson, R.M., Godt, J.W., Logan, M., and Solovits, S.A. 2015. "Controls on the Breach Geometry and Flood Hydrograph During Overtopping of Noncohesive Earthen Dams". *Water Resour. Res.,* 51, 6701–6724, doi:10.1002/2014WR016620.

Association of State Dam Safety Officials. 2022. "Dam Failures and Incidents" Accessed November 8, 2022. https://stag.damsafety.org/dam-failures

U.S. Army Corps of Engineers. 2021. "National Inventory of Dams" Accessed November 8, 2022. https://nid.sec.usace.army.mil/#/

APPENDIX A: TABLES

EXPERIMENT NUMBER	DAM HEIGHT (CM)	GRAIN SIZE	OTHER INFO
1	10	100% SAND	
2	15	100% SAND	
3	20	100% SAND	
4	30	100% SAND	
5	45	100% SAND	
6	15	10% SILT	
7	20	10% SILT	
8	30	10% SILT	
9	15	25% SILT	
10	20	25% SILT	
11	30	25% SILT	
12	15	100% SAND	LARGER RESERVOIR
13	15	100% SAND	5 BLOWS COMPACTION
14	15	100% SAND	20 BLOWS COMPACTION
15	15	100% SAND	30 BLOWS COMPACTION
16	30	100% SAND	REPEATED
17	20	100% SAND	REPEATED
18	20	100% SAND	REPEATED
19	15	25% SILT	REPEATED
20	15	10% SILT	REPEATED

Table A.1: A list of the experiments whose results are presented in this paper, including the experiment number, the dam height, the sediment mixture and other important information. Experiments 1 – 11 are presented in the results section. Experiments 12 – 20 are additional experiments are used to address assumptions such as reservoir size, compaction as well as repeatability.

Experiment #	End of Phase 1	End of Phase 2	Bank Failures	Platform Exposed	Peak Discharge	Bank Failures	End of Experiment
1	23	77	164	224	265		340
2	46	91	157	178	206	220	280
3	57	78	193	193	192	287	290
4	172	180	248	277	300	327	400
5	191	208	266	288	305	330	440
6	16	138		190	237	238	320
7	14	223	285	292	312	332	450
8	14	162			257	329	345
9	24	236		318	350	388	440
10	12	235		300	319 & 430		480
11	21	283	332	374	419		500

Table A.2: Displays the time that phases 1 and 2 end in all experiments as well as the time of significant breach events such as peak discharge, the platform being exposed and bank failures occurring.

	Bulk Density (g/cm^3)		
Number of Compaction Blows	100% Sand	10% Silt	25 % Silt
5	1.44	1.53	1.77
10	1.58	1.60	1.88
15	1.65	1.65	1.94
15 (5 blows, 3 layers)	1.66	1.76	2.05
30	1.65	1.73	2.03
30 (15 blows, 2 layers)	1.61	1.65	1.95

Table A.3: Results of bulk density tests, with varying compaction amounts and method of compaction.

APPENDIX B: FIGURES

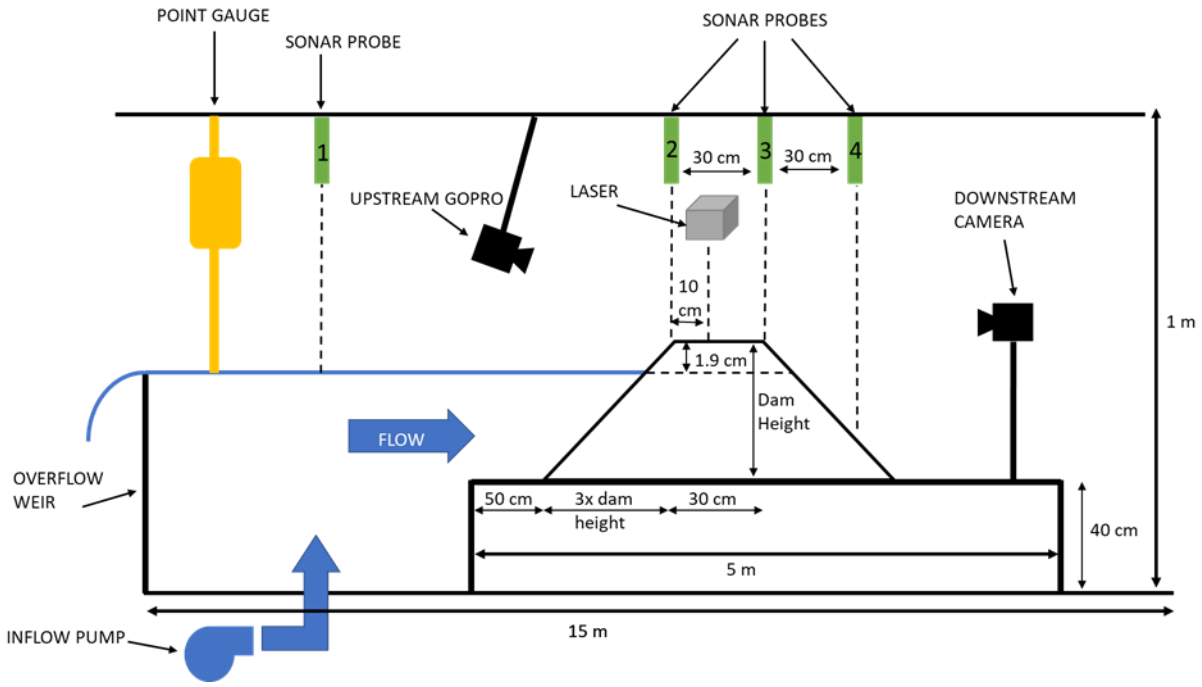

Figure B.1: A schematic of the experimental set up. Including dam and flume dimensions, measurement devices as well as the inflow pump and overflow weir.

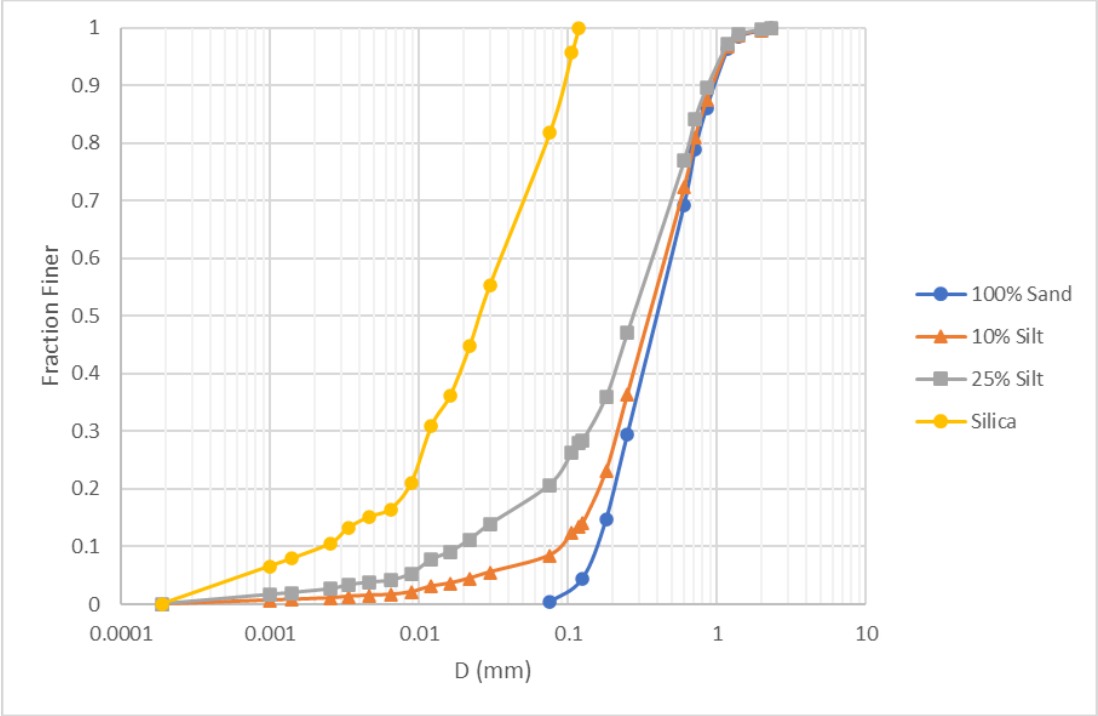

Figure B.2: Grain size distributions of sediment mixtures used in experiments, including the grain size distribution of the silica used to create mixtures.

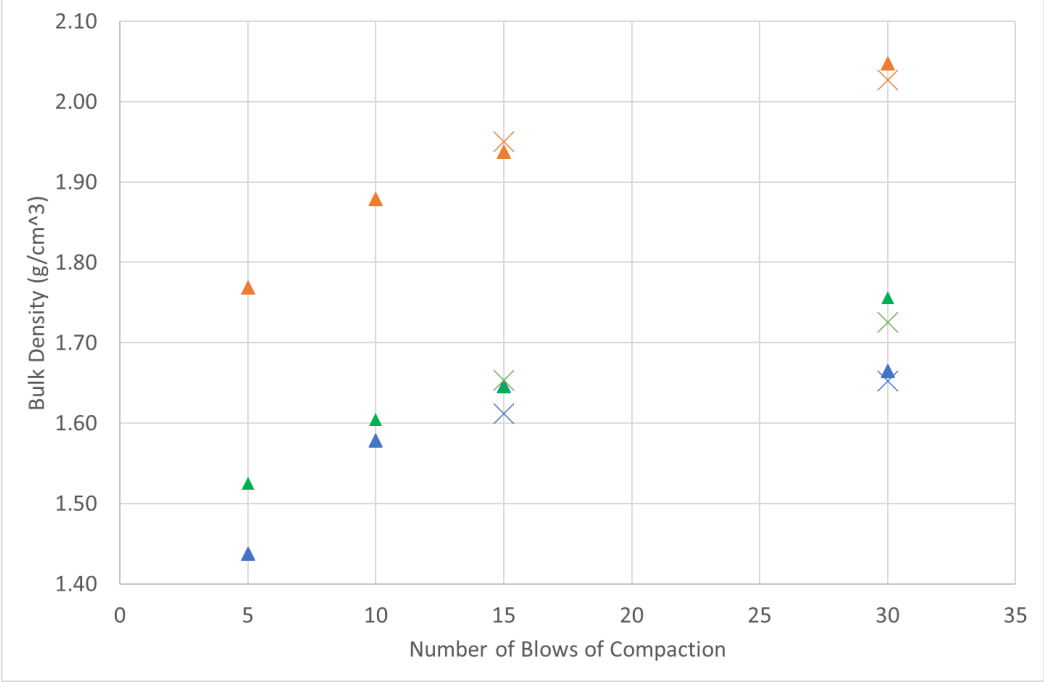

Figure B.3: Bulk Density of the three grain size distributions plotted against the number of compaction blows, where blue is 100% sand, green is 10% silt content and orange is 25% silt content. Triangles represent tests with number of blows on one layer. Xs are tests where the cumulative blows of multiple layers, with 5 blows on three layers results in 15 cumulative blows and 15 blows on two layers results in 30 cumulative blows.

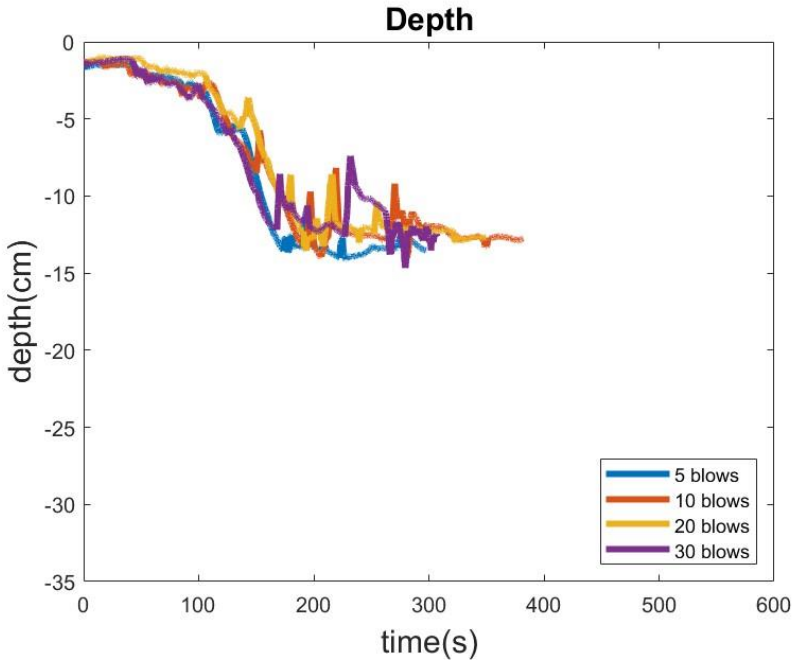

Figure B.4: The temporal evolution of incision process in 15 cm dams with varying amounts of compaction. The impact of compaction is not included in the results section of this paper, however, is considered in the discussion section.

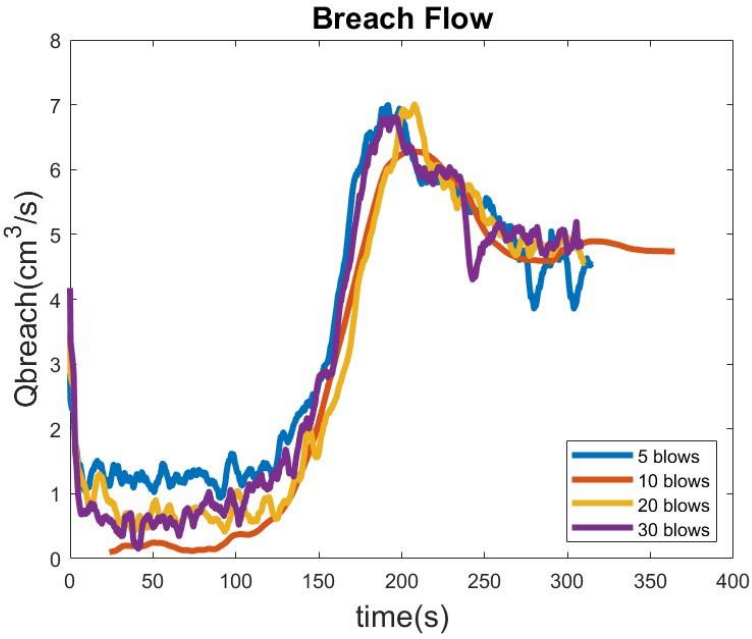

Figure B.5: The breach hydrographs in 15 cm dams with varying amounts of compaction. The impact of compaction is not included in the results section of this paper, however, is considered in the discussion section.

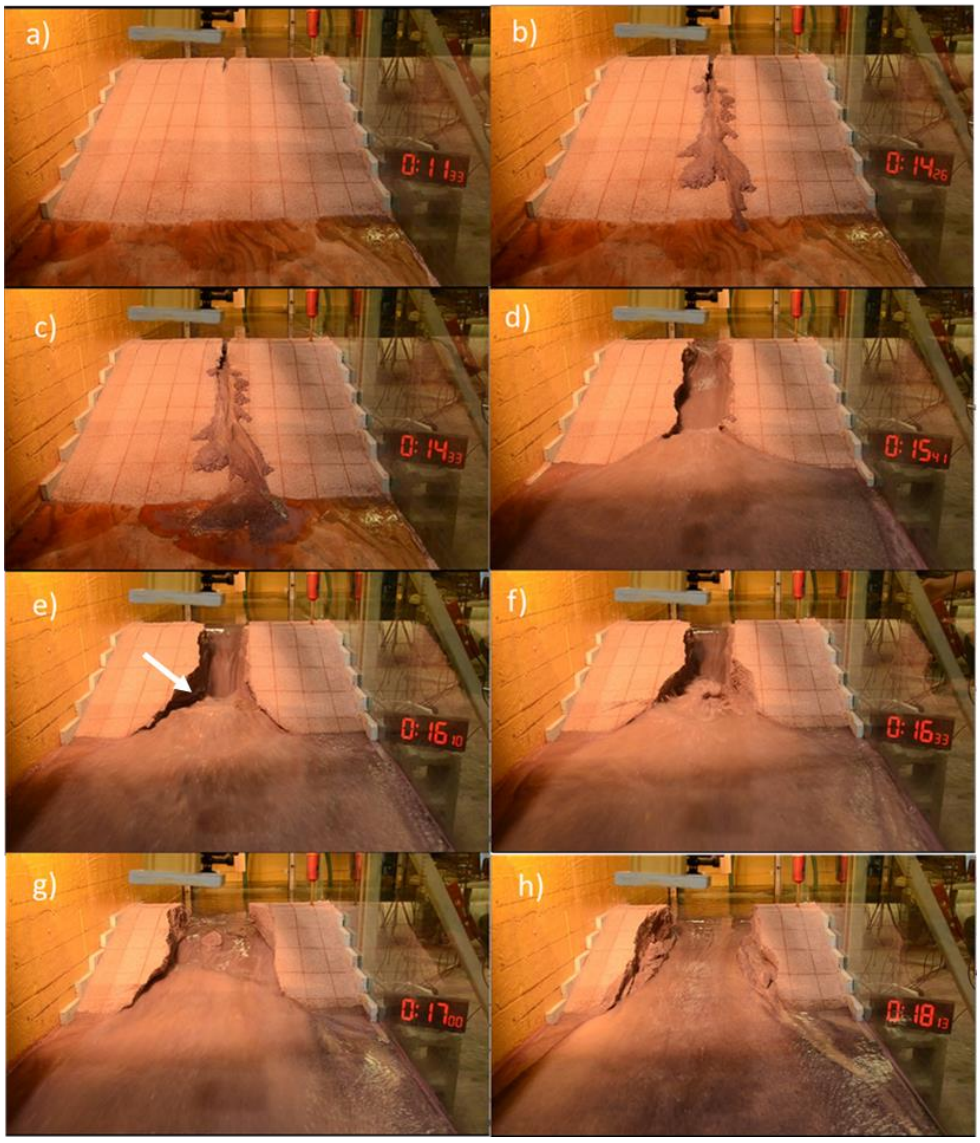

Figure B.6: Breach evolution of a 30 cm sand dam. Frame a represents time equal to 0 when water is entering the channel. Frame b represents the time that water reaches the dam toe (t = 174s) and concludes the first phase of breaching, this frame shows the sediment deposition that occurs on the downstream face. Frame c is the time when the upstream dam crest begins eroding which concludes the second phase of the breach (t = 180s). Frame d shows channel widening after minor bank failures had recently occurred (t=248s). Frame e is at time=277s at which point the platform had been exposed due to a scour hole just upstream of the dam toe. Frame f shows the time at which the peak discharge occurs (t=300s). Frame g again shows channel widening that has occurred due to major bank failures (t=327s). Lastly frame h shows the end of the experiment at t = 400s.

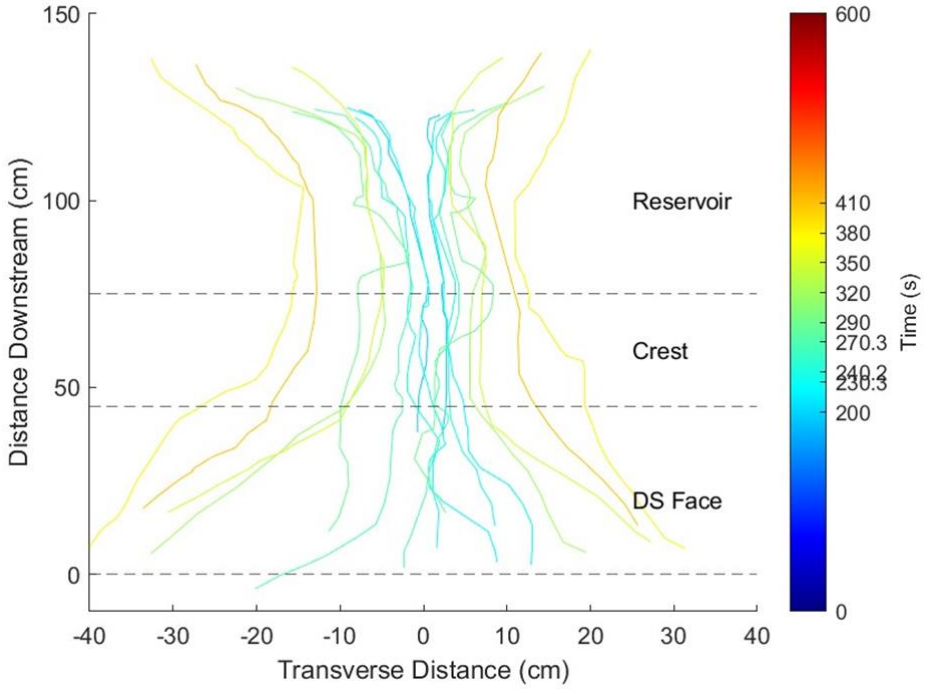

Figure B.7: Breach channel width change for a 30 cm dam with 100% sand content, where each line is a time represented through the color bar on the right.

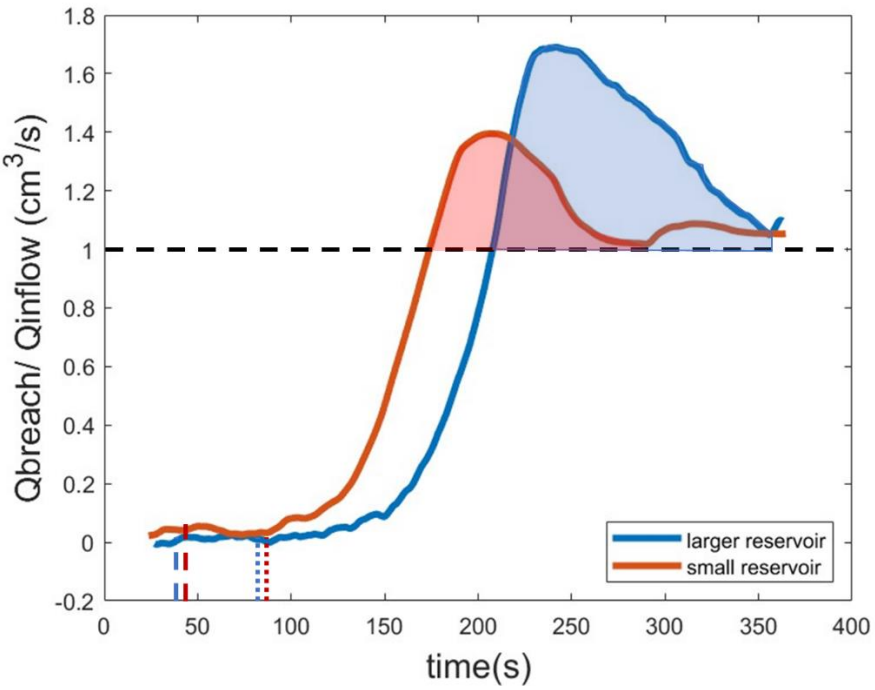

Figure B.8: Nondimensional breach hydrograph of two 15cm dams, where the red line represents the dam with a smaller reservoir and the blue line has a larger reservoir. The horizontal dashed line is equal to 1 on the y axis, this is where the discharge through the breach is equal to the inflow discharge. The area above this line shows the impact due to

reservoir size. The dashed vertical lines signify the time that phase 1 ends, and the dotted vertical lines signify the time that phase 2 ends.

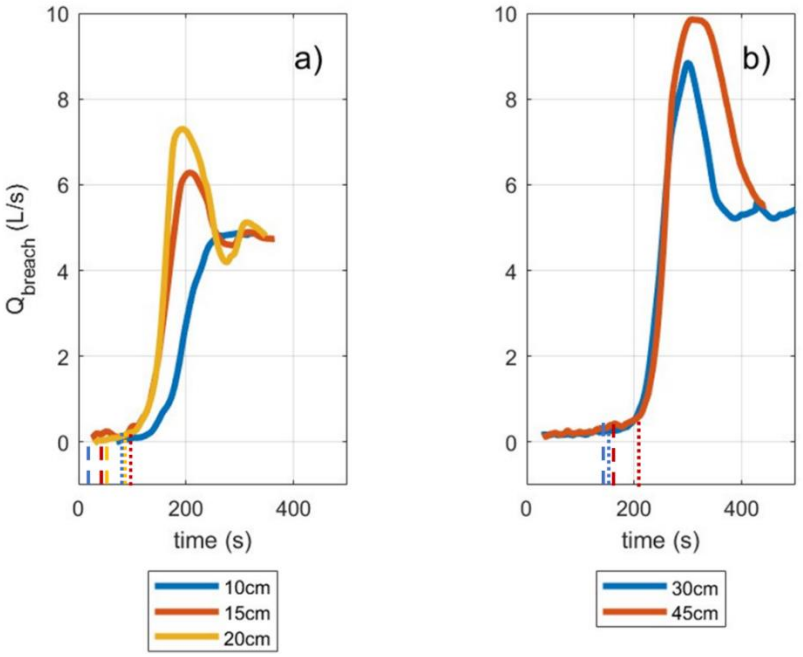

Figure B.9: Breach hydrograph for small dams in panel a and for large dams in panel b. The dashed vertical lines represent the end of phase 1, while the dotted vertical lines represent the end of phase 2.

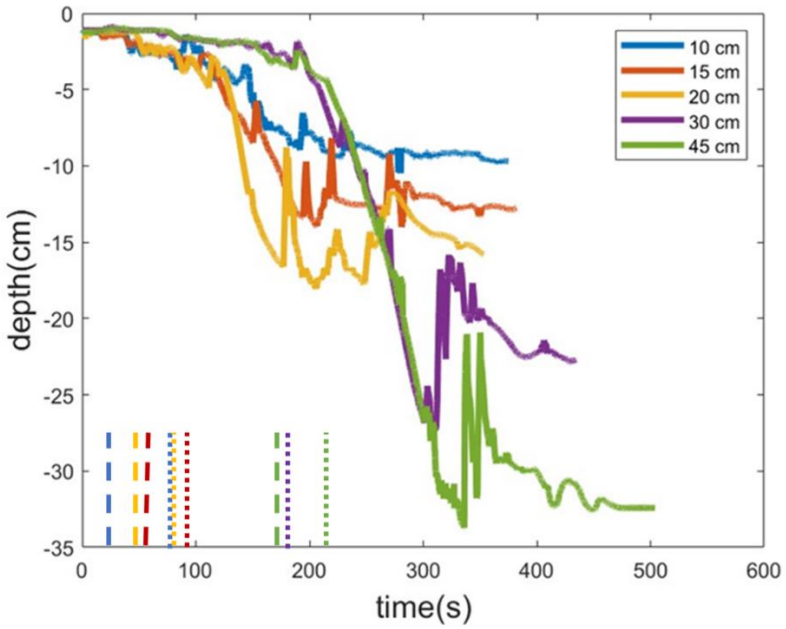

Figure B.10: The temporal evolution of depth measurements on the dam crest for all dam heights of sand dams at a cross sectional location 10 cm upstream of the downstream crest. The y axis is the depth measurements where 0 is the elevation of the dam crest and all negative measurements are the depth eroded below the dam crest. Spikes in the graph

are caused by bank failures in the channel. The dashed vertical lines represent the end of phase 1, while the dotted vertical lines represent the end of phase 2.

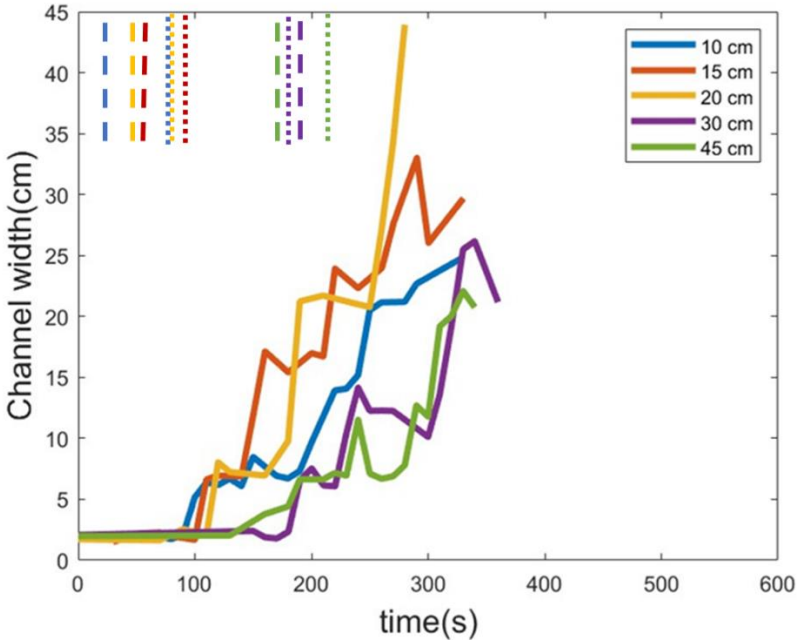

Figure B.11: Temporal evolution of channel width measurements for all dam heights of sand dams measured on the dam crest, specifically 10 cm upstream of the downstream dam crest. The y axis is the computed channel width where 2 cm is the initial pilot channel on the dam crest. The dashed vertical lines represent the end of phase 1, while the dotted vertical lines represent the end of phase 2.

Figure B.12: The breach evolution of a 30 cm, 25% sand-silt dam. Frame a represents time equal to 0 when water is entering the channel. Frame b represents the time that water reaches the dam toe and concludes the first phase of breaching, this frame shows there is no sediment deposition on the downstream face (t=21s). Frame c shows the erosional waves developing along the downstream dam face (t=119s). Frame d is the time when the upstream dam crest begins eroding which concludes the second phase of the breach (t=283s). Frame e shows channel widening near the dam toe that has occurred due to minor bank failures (t=332s). Frame f again shows channel widening which is now occurring further upstream due to bank failures, it is at this point that erosion below the dam top surface is occurring causing overhanging banks (t=374s). Frame g shows the

time that the peak discharge occurs (t=419s). Lastly frame h shows the final breach geometry at the end of the experiment (t = 500s).

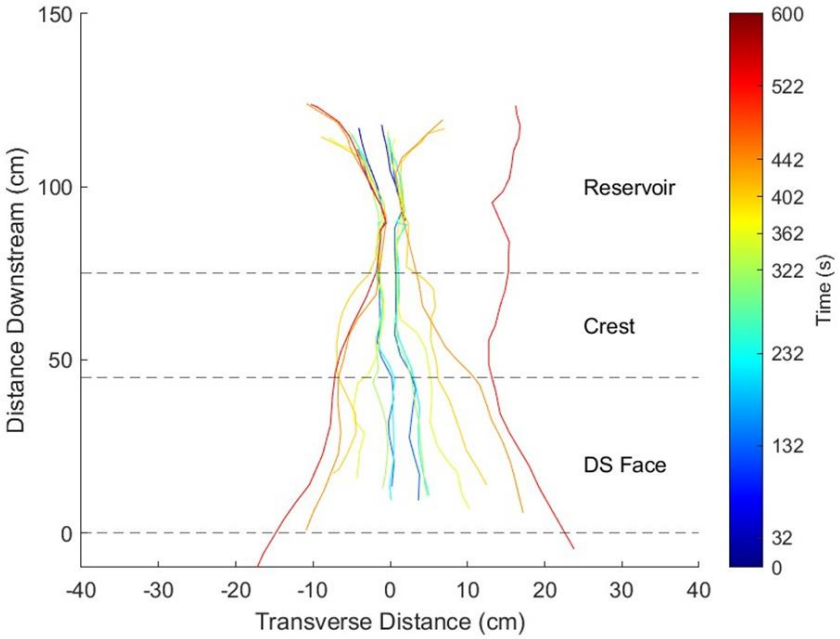

Figure B.13: Breach channel width change for a 30 cm dam with 25% silt content, where each line is a time represented through the color bar on the right.

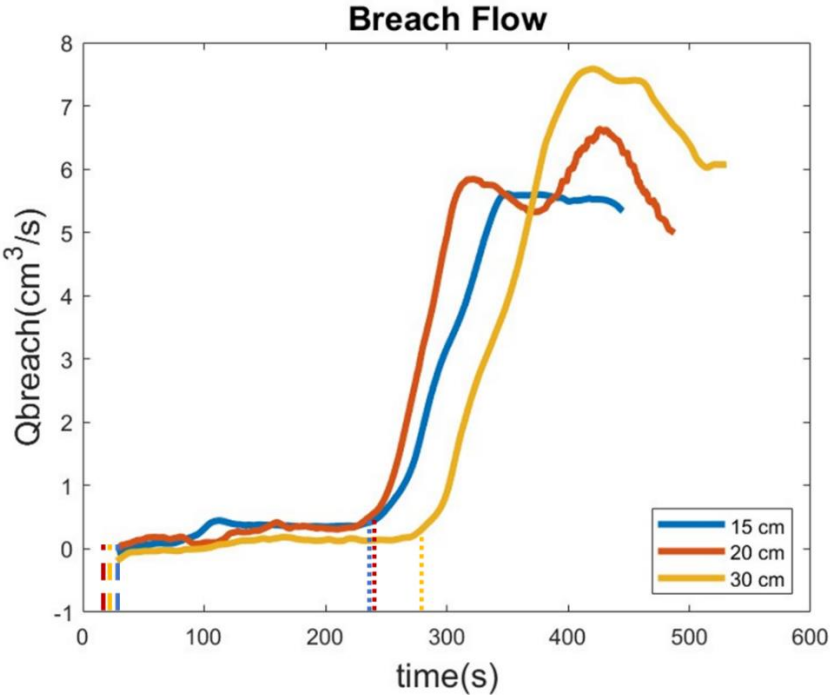

Figure B.14: Breach hydrographs for the 25% sand-silt dams. The 20cm dam hydrograph has two peaks caused by a major bank collapse occurring. It is reasonable to assume that in the absence of bank failure, the peak of the 20 cm dam experiment would fall between the peaks of the 15 cm and 30 cm dam experiments for both time and magnitude. The

dashed vertical lines represent the end of phase 1, while the dotted vertical lines represent the end of phase 2.

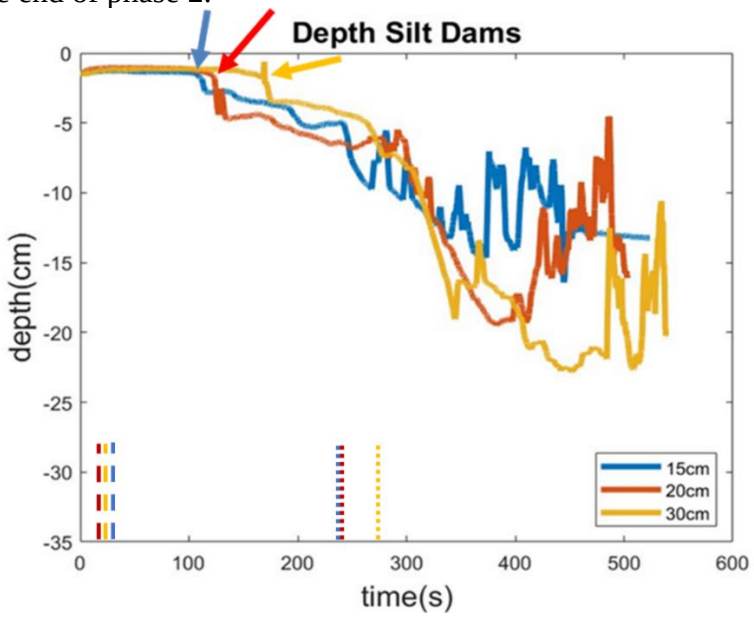

Figure B.15: Temporal evolution of depth measurements on the dam crest for all dam heights of 25% concentration sand-silt dams at a cross sectional location 10 cm upstream of the downstream crest. The y axis is the depth measurements where 0 is the elevation of the dam crest and all negative measurements are the depth eroded below the dam crest. Spikes in the graph are caused by bank failures in the channel. The dashed vertical lines represent the end of phase 1, while the dotted vertical lines represent the end of phase 2.

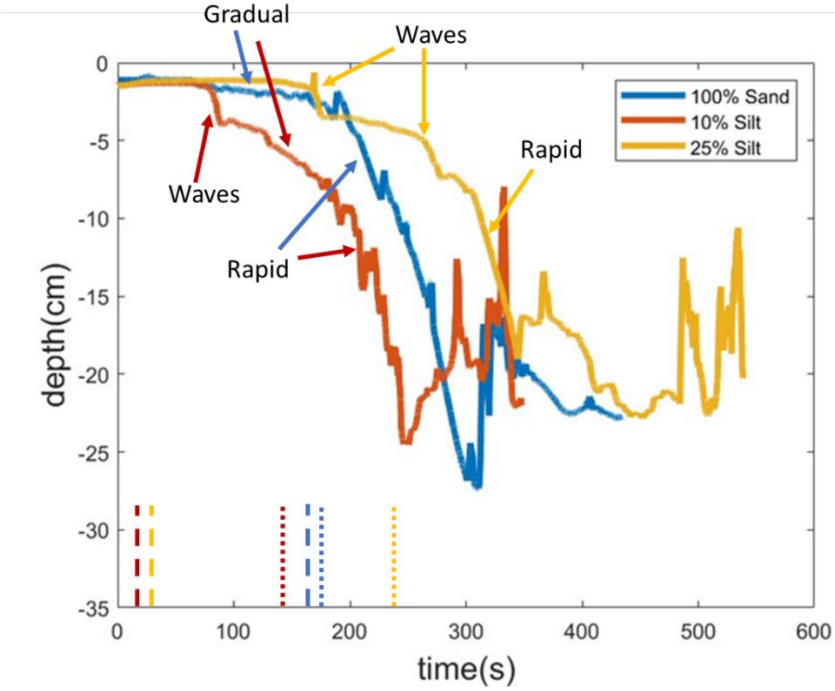

Figure B.16: Temporal incision on the dam crest for 30 cm dams of all three sediment mixtures. The dashed vertical lines represent the end of phase 1, while the dotted vertical lines represent the end of phase 2.

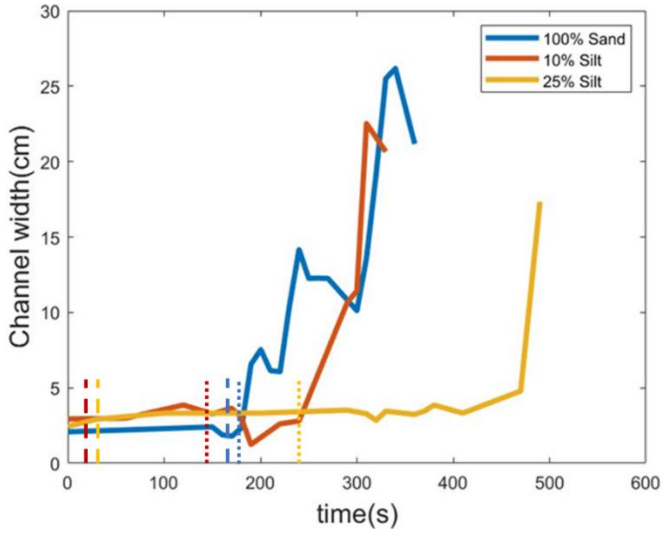

Figure B.17: Temporal channel width for 30 cm dams of all three sediment mixtures. The dashed vertical lines represent the end of phase 1, while the dotted vertical lines represent the end of phase 2.

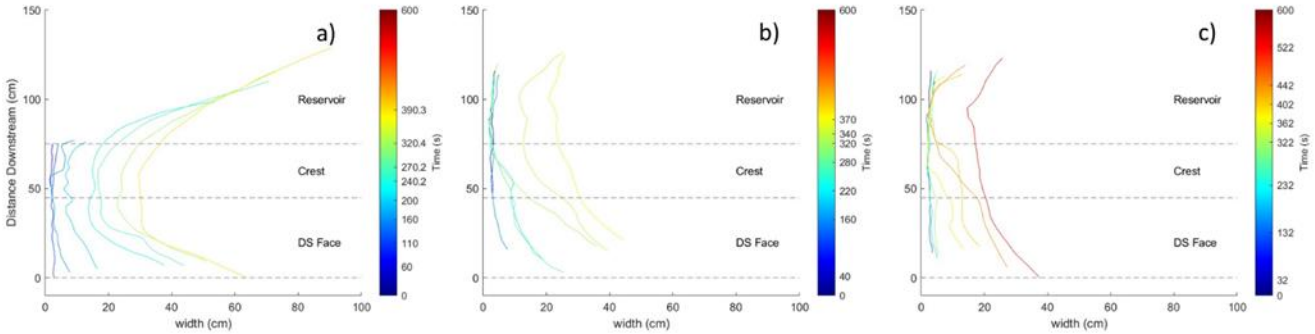

Figure B.18: Breach channel width change for three 30cm dams, where each line is a different time during the experiment represented through the color bar. Frame a is 100% sand content, frame b is 10% silt content and frame c is 25% silt content.

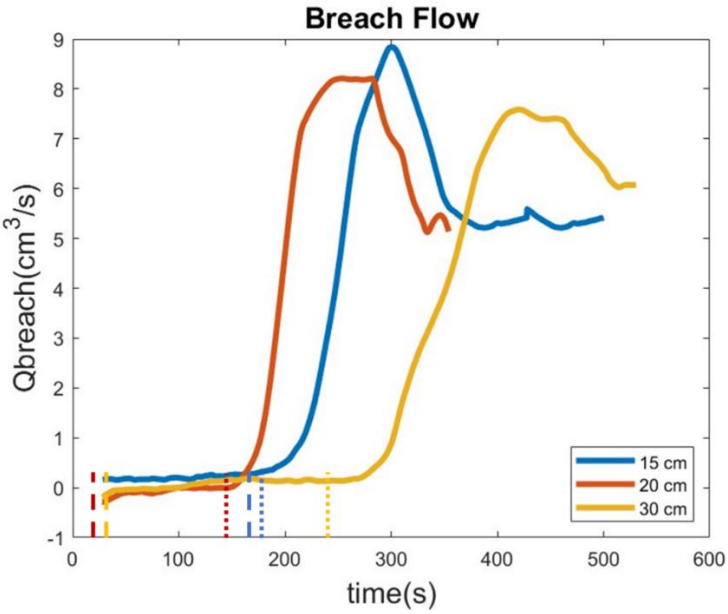

Figure B.19: Breach hydrographs for 30 cm dams of all three sediment mixtures. The dashed vertical lines represent the end of phase 1, while the dotted vertical lines represent the end of phase 2.

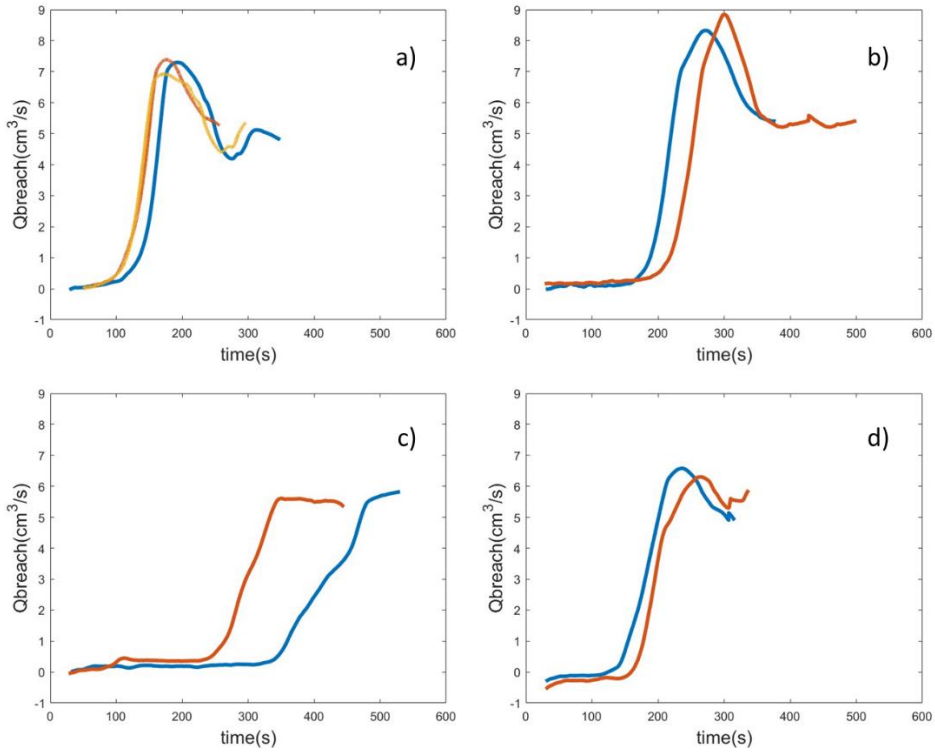

Figure B.20: Nondimensional breach hydrographs of all repeatability experiments where frame a shows three 20 cm dams of 100% sand, frame b shows three 30cm dams of 100% sand, frame c shows two 15cm dams of 25% silt and lastly frame d shows two 15cm dams of 10% silt.

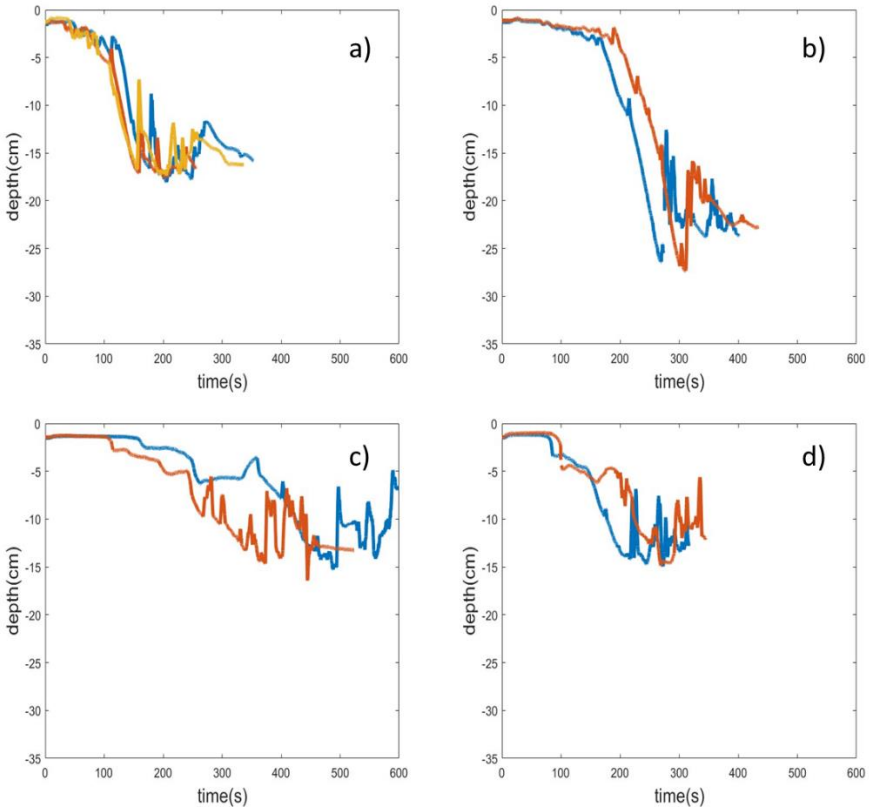

Figure B.21: Time evolution of incision in all repeatability experiments where frame a shows three 20 cm dams of 100% sand, frame b shows three 30cm dams of 100% sand, frame c shows two 15cm dams of 25% silt and lastly frame d shows two 15cm dams of 10% silt.